ACS APPLIED MATERIALS & INTERFACES

Research Article

www.acsami.org

Formation of Gradient Multiwalled Carbon Nanotube Stripe Patterns by Using Evaporation-Induced Self-Assembly

Liang Xiao,[†] Jiali Wei,[†] Yong Gao,*[,†] Duanguang Yang,[†] and Huaming Li*[,†,‡]

[†]College of Chemistry and [‡]Key Laboratory of Polymeric Materials & Application Technology of Hunan Province, Key Laboratory of Advanced Functional Polymeric Materials of College of Hunan Province, and Key Lab of Environment-Friendly Chemistry and Application in Ministry of Education, Xiangtan University, Xiangtan 411105, Hunan Province, P. R. China

ABSTRACT: Gradient stripe patterns of multiwalled carbon nanotubes (MWCNTs) with remarkable regularity over large areas were fabricated by using evaporation-induced self-assembly technique. In this method, a glass coverslip was inclinedly immersed into a suspension of MWCNTs in dichloroethane. By controlling the solvent evaporation temperature, well-defined gradient stripes were formed at the air−solvent−substrate contact line. The effects of several experimental parameters, such as the substrate tilt angle, concentration of MWCNTs, and evaporation temperature, on the regularity of stripes were discussed. A possible stripe formation process was described as a negative feedback of MWCNT concentration caused by a concavely curved shape of the meniscus. Additionally, the strips of MWCNTs on Si/SiO_2 substrate were directly used to fabricate field-effect transistor (FET) devices. The electrical properties of the MWCNT-FET devices were also investigated.

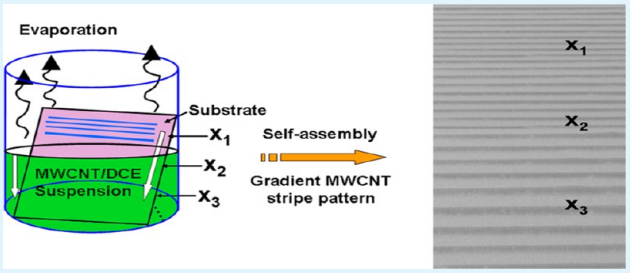

KEYWORDS: *gradient stripe, pattern, mutiwalled carbon nanotubes, evaporation, self-assembly, field-effect transistor*

INTRODUCTION

Because of the unique structural and electronic properties of carbon nanotubes (CNTs), they have been investigated for numerous applications that include microelectronics,[1−4] sensors,[5−7] and field-emission devices.[8−11] Although some of these applications can be realized through in situ growth,[12−15] many others will require organization strategies that controllably deposit CNTs in desired locations with nanoscale dimensions over a large area.[16−20] Therefore, the selective assembly of CNTs on substrates offers further possibilities for the parallel fabrication of large-scale CNT electronics. Recently, two main manipulation techniques including in situ synthesis[21−24] and postsynthesis treatment[25−31] have been developed for the deposition or patterning of CNTs onto substrates, in which the in situ synthesis involves direct CNTs growth on catalytic templates, while the postsynthesis treatment involves depositing of suspended CNTs in solution onto a prepatterned substrate. Although the latter method may be time-consuming and complex, the postassembly process of prefabricated tubes implies advantages, as the usually harsh synthesis conditions can be omitted. As a result, the method serves to expand the number of possible applications and can also be applied on substrates that are incompatible with these conditions.[27,32−34] Additionally, the postprocessing of as-grown CNTs has allowed CNTs to be controlled in length, purified, modified with functional groups, dispersed in desired solvents, and eventually patterned on substrate with high resolution.[35−37]

Recent developments of postsynthesis techniques to deposit or pattern CNTs are classified into three main categories: chemical methods, physical methods, and external field methods. Generally, chemical approaches rely on covalent bonds or noncovalent interactions to attach and pattern the functionalized CNTs to the prepatterned surface.[38,39] Physical methods heavily depend on physical forces to deposit the CNTs. For example, printing[26,40,41] and lithography techniques[1,42,43] are highly suited for patterning CNTs and are typically quite fast and simple. But the resolution is limited due to the stamp or mask distortion, whereas the lifetime and reproducibility are unproven. The external field methods rely on the electric[18,44] or magnetic field forces[45] to place CNTs. However, successful implementation of CNTs also requires alternative strategies to deposit and pattern CNTs over large areas, especially if gradient variation of patterning (e.g., stripe width) is desirable.

Recently, gradient concentric rings of CNTs over large surface areas have been successfully produced by combining two consecutive self-assembly processes, namely, spontaneous evaporation-induced self-assembly of polymers in a sphere-on-flat geometry, followed by subsequent directed self-assembly of CNTs on the polymer-templated surfaces.[29] Additionally, self-organized ribbons of aligned CNTs have also been fabricated by drying mediated self-assembly process at 100 °C.[46] The self-organization of the aligned nanotube ribbons was interpreted as relating to two factors: oxidization of the CNTs and prolonged heating of the CNTs aqueous suspension. The oxidation of CNTs with strong acid results in the introduction of hydroxyl

Received: February 19, 2012
Accepted: July 6, 2012
Published: July 6, 2012

and carboxyl groups on the surface of CNTs, which can play a bonding role between the CNTs to form the ribbons. Heating the suspension may provide the driving force for alignment of the nanotubes. Without heating the suspension, the CNTs cannot self-align. Indeed, a continuous CNTs film was formed on the substrate when a room temperature dip-coating technique was used.[47] In this method, a hydrophilic glass slide was vertically immersed into an aqueous dispersion of acid-treated CNTs. As the water gradually evaporated, the CNTs were observed to assemble only along the air−liquid-substrate triple line of the glass surface. A continuous CNTs film was formed when the water was completely evaporated. By combining the substrate prepatterning techniques, this dip-coating procedure was suitable to fabricate CNT patterns with uniform surface coverage. However, this method relies heavily on prepatterned substrate. Moreover, it can be time-consuming, expensive, complex, and reproducibility may be difficult to ensure. On the other hand, CNT patterns can also be constructed by the evaporation-driven self-assembly of non-covalently functionalized CNTs in aqueous solution. For example, CNT superlattice structure with good alignment was produced by this self-assembly method.[48] In this case, 99% purity semiconducting arc-discharge CNTs suspended in 1% sodium dodecyl sulfate (SDS) aqueous solution, with a diameter range $1.3 < d < 1.7$ nm, was used for assembly. But the mechanism for the large scale alignment of the nanotube superlattice remains unclear. In addition, lattice-like pattern of CNTs from evaporation of aqueous droplets of CNTs coated with a physisorbed layer of humic acid (HA) in special geometries of the substrate surfaces has very recently been reported by Zeng and co-workers.[49] It was found that the substrate surface geometry played an important role in the pattern formation of CNTs. Ordered lattice-like patterns with filaments of CNTs in both parallel and perpendicular to the boundary line of the evaporating droplet were obtained after evaporation of CNT dispersion in wedge and curved-wedge configurations. Conversely, no ordered structure was formed on the flat substrate surface geometries. A detailed explanation of the formation of the resulting patterns was proposed on the basis of two competing or cooperative sedimentation mechanisms: (1) capillary forces between CNTs giving micrometer-sized filaments parallel to the boundary line of the evaporating droplet and (2) fingering instability at the boundary line of the evaporating droplet and subsequent pinning of CNTs on the surface giving micrometer-sized filaments of CNTs perpendicular to this boundary line. Unfortunately, these fabrication approaches need to introduce small organic molecules to the self-assembly system, which are difficult to be removed from the CNT patterns. The incorporation of organic additives induces heterogeneous impurities and is detrimental to the properties of CNTs, thus limiting their applications. Therefore, it remains a great challenge to develop simple and straightforward methods (without any additives) for the fabrication of CNT patterns.

In the present work, we constructed gradient stripe patterns of multiwalled carbon nanotubes (MWCNTs) over large areas using a simple and straightforward self-assembly technique. In this method, a glass coverslip was inclinedly immersed into a suspension of MWCNTs in 1,2-dichloroethane (DCE). By controlling the solvent evaporation temperature, well-defined stripes having a gradient width were spontaneously formed on the glass substrate. The gradient in stripe widths was determined by the progressively increased concentration of MWCNTs in the suspension as the solvent was gradually evaporated, because the MWCNT concentration determined the MWCNTs supplied to the stripe growing region, which was therefore related to the stripe width. Meanwhile, the substrate should be tilted at an angle to horizontal to guarantee the gradient characteristic of the self-assembled MWCNT stripes.

EXPERIMENTAL SECTION

Materials. The MWCNTs with a diameter of 10−20 nm and a length of ca. 5−15 μm, produced by chemical vapor deposition (CVD) method, were purchased from Chengdu Institute of Organic Chemistry (Chinese Academy of Science). The raw materials were purified by refluxing in 2.6 M HNO_3 for 12 h and filtering under vacuum. The structure of MWCNTs remains basically intact after mild acid treatment as evidenced by Raman spectroscopy and thermogravimetric analysis (TGA). As shown in Figure 1, the as-received and acid

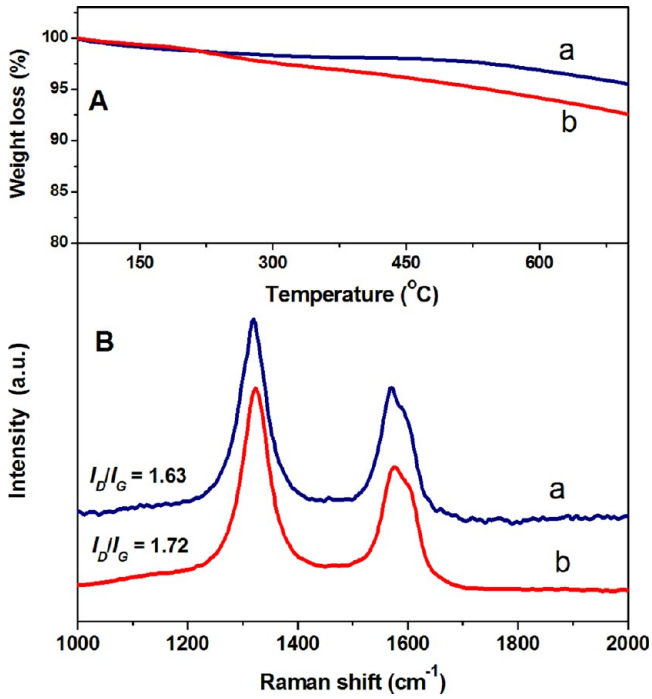

Figure 1. (A) TGA curves and (B) Raman spectra of (a) as-received MWCNTs and (b) 2.6 M nitric acid treated MWCNTs.

treated MWCNT samples show very little change in their Raman spectra. For example, the intensity ratio between Raman D and G bands (I_D/I_G) is found to be 1.63 and 1.72, respectively, for MWCNTs before and after purification, which is a clear indication that the nanotube structure, as a whole, remains almost intact. Supporting evidence comes from TGA analysis, only minor mass loss (<3 wt %) is observed for acid-treated MWCNTs below 500 °C if the mass loss of the as-received MWCNTs is used as the reference. Such minor lose may be attributed to decarboxylation and elimination of hydroxyl functionalities. The purified MWCNTs can be well-dispersed in DCE. After separation by centrifugation at 4250 g for 30 min, a homogeneous suspension was stabilized up to 100 mg/L without flocculation for several weeks.

The glass coverslips (18 × 18 mm^2) were first washed with detergent and then boiled in 80 °C piranha solution (3/1, 98% sulfuric acid and 30% hydrogen peroxide) for 10 min to remove the organic contaminants. Afterward, the substrates were ultrasonicated in acetone, absolute ethanol, and deionized water for 10 min, respectively, and blown dry with a stream of nitrogen. The Si/SiO_2 substrates (15 × 15 mm^2) were purchased from Shanghai Institute of Optics and Fine Mechanics (Chinese Academy of Sciences).

Fabrication of Stripe Patterns. Figure 2 illustrates a schematic of the experiment setup. In a typical procedure, a glass vessel (10 mL beaker, diameter = 25 mm) containing a MWCNT/DCE suspension with the given concentration (i.e., 2, 10, 20, 100 mg/L) was preheated in a water bath to the temperature that was corresponding to the internal temperature T_i of the incubator. The beaker was uncovered and a cleaned glass coverslip was immersed into the suspension with the tilt angle set as 45, 60, or 90°. Subsequently, the liquid level was adjusted to the same plane with the upper edge of the substrate and the vessel was carefully placed into the incubator. The evaporation rate was varied in a range of 9.0−21.0 μL/min by changing the temperature from 40 to 70 °C.

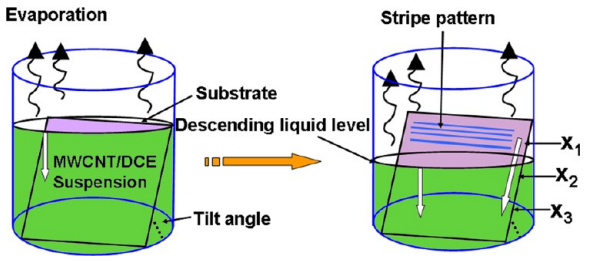

Figure 2. Schematic illustration of the experimental setup. X_1, X_2, and X_3 are the distances of stripes away from the uppermost edge of the substrate at uppermost region (X_1), intermediate region (X_2), and bottommost region (X_3), respectively.

In a second experiment, the above procedure was repeated, but the substrate was replaced by Si/SiO_2 plate for the purpose of fabricating MWCNT-based field-effect transistor (FET) devices. The internal temperature T_i and substrate tilt angle were maintained at 60 °C and 45°, respectively, while the concentration of MWCNT/DCE suspension was varied from 2.0 to 10 mg/L. The strips of MWCNTs produced at a MWCNT concentration of 5.0 mg/L were subsequently used to fabricate MWCNT-FET devices.

Fabrication of MWCNT-FET Devices. After the MWCNT self-assembly process, the produced MWCNT stripes were rinsed in ethanol, followed by thermal treatment at 120 °C for 2 h. Two platinum electrodes were sputter deposited and defined as the source and drain electrodes using a metal maskplate. The Si/SiO_2 substrate is a highly doped p-type substrate that can be used as a back gate. The total area of the metal maskplate is 1 cm^2 and the areas of source and drain are both 4.5 mm^2. The channel length and width of the FETs are 200 and 1500 μm, respectively. Before measurements, the as-fabricated MWCNT-FETs were rapidly annealed at 400 °C for 2 min.

Characterization. The morphology and regularity of the stripe patterns were observed by optical microscopy (Leica DM4500 P, Germany). Prior to imaging, the CNTs deposited on the backside of the substrate were slightly washed away with absolute ethanol for the purpose of interference elimination. A field emission scanning electronic microscope (SEM) (Hitachi, S-4800) was used to observe the microscopic structure of the stripes. Electrical properties of MWCNT-FETs were measured using a Keithley 4200-SCS semiconductor parameter analyzer.

RESULTS AND DISCUSSION

Formation of Gradient MWCNT Stripe Patterns. To fabricate gradient MWCNT stripes over a large area, the hydrophilic coverslip was inclinedly immersed into the MWCNT/DCE suspension. At first the substrate was set at a tilt angle of 45°. Figure 3 shows typical SEM images of gradient stripes fabricated from the evaporation-mediated self-assembly of a 10 mg/L MWCNT/DCE suspension at 50 °C. As shown in Figure 3a, gradient MWCNT stripes with remarkable regularity over a large area were formed. The entire stripe pattern was formed over 300 mm^2 surface area with relatively high uniformity (Figure 3h). It is worth noting that the stripe width increased with increased proximity to the bottom of the substrate (i.e., from X_1 to X_3), which can be attributed to the

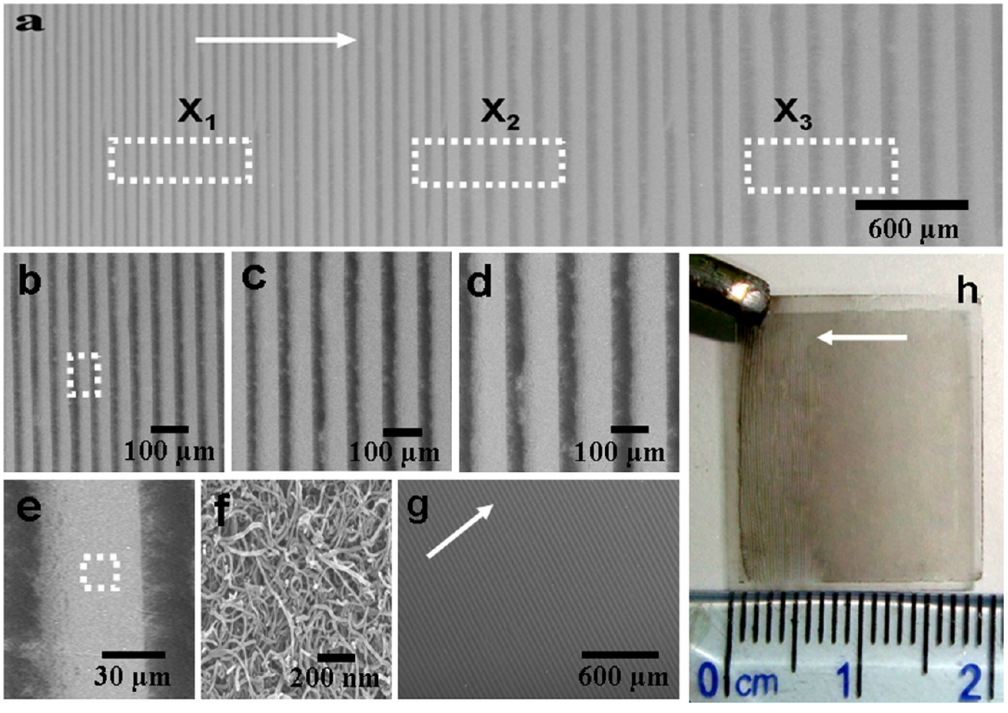

Figure 3. (a) Representative SEM image of the gradient stripe pattern formed from MWCNT/DCE suspension (10 mg/L) at T_i = 50 °C with the substrate tilt angle of 45°. (b−d) Magnified images of marked zones at region X_1, X_2, and X_3 in a. (e, f) Magnified images of marked zones in b and e. (g) Regular stripes on vertical substrate at region X_1. The white bands are MWCNTs stripes and the white arrows indicate the direction of stripe growth. (h) Photograph of MWCNT stripe pattern on the glass substrate.

gradual increase of nanotube concentration in the MWCNT/DCE suspension. At the uppermost region, stripe width increased progressively from 52 μm ($X_1 \approx 4.0$ mm in Figure 3b) to 78 μm at the intermediate region ($X_2 \approx 8.0$ mm in Figure 3c) to 106 μm at the bottommost region ($X_3 \approx 12$ mm in Figure 3d), as determined by SEM. On the other hand, the stripe spacing also had an increasing tendency. Through a careful observation of Figure 3e, the white band was a nanotube stripe, in which MWCNTs formed random network and were densely packed as shown in the magnified image of the stripe (Figure 3f). The gray band indicated a bare part of the substrate where trace MWCNTs was deposited. Conversely, the gradient characteristic of the stripe width vanished when the substrate was vertically immersed into the MWCNT/DCE suspension. The stripe width was almost constant as shown in Figure 3g.

Recently, Miyahara and co-workers[50] have presented detailed reliability studies for mechanism of stripe pattern formation on hydrophilic surfaces by using convective self-assembly. In their method, a substrate immersed in aqueous suspension of colloidal silica sphere was withdrawn vertically at a controlled temperature. It was found that well-defined stripes were spontaneously formed at the air−solvent−substrate contact line. They demonstrated that the stripe formation is neither a stick−slip motion of the contact line nor dewetting but a negative feedback of particle concentration caused by a concavely curved shape of the meniscus. Based on their arguments, a similar mechanism for stripe formation is thus proposed. In our case, a meniscus can also form a concave surface against the substrate because its top edge can be attached to the outermost layer of entangled nanotubes. As the solvent is evaporated, the meniscus is elongated and concavely curved. After a certain time, the elongation of meniscus stops and cut off from the bulk suspension at a threshold, leading to the formation of stripe and spacing. Notably, the meniscus is more elongated on the inclined substrate than that on the vertical one, resulting in a wider spacing as well as a wider stripe. On the other hand, the concentration of MWCNTs in the suspension increased progressively as the solvent was gradually evaporated, although a small portion of the MWCNTs was self-assembled on the substrate as well as on the wall of the container. In order to verify this, the variation of MWCNT concentration in the residual suspension was monitored by UV−vis spectroscopy. The specific extinction coefficient of MWCNTs is found to be 0.0145 L/mg/cm at 500 nm[51] and can be used to estimate the concentration of nanotube suspensions. As shown in Figure 4, the concentration of residual MWCNTs in the suspension almost increased linearly with gradual evaporation of the solvent. Because the MWCNT concentration determines the MWCNTs supplied to the stripe growing region, which is therefore related to the stripe width.

Previous studies have also demonstrated that the stripe width increased almost linearly against the solute concentration.[49,52] Because of the gradient variation of the nanotube concentration, gradient MWCNT stripes were thus achieved, as illustrated in Figure 3. This assembly method provides an opportunity to control the concentration of nonvolatile solutes (i.e., nanotube) when the bulk suspension is evaporated, which in turn regulates the structure formation. Therefore, in contrast to the continuous CNTs film formed on the substrate via room temperature dip-coating technique, ordered and gradient stripes of nanotube were produced using this drying-mediated self-assembly method. Furthermore, this simple and straightforward

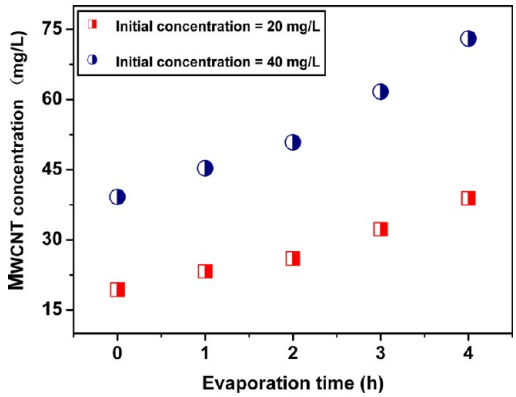

Figure 4. Variation in MWCNT concentrations in the residual suspension as a function of evaporation time.

method, which dispenses with the need for CNTs functionalization (i.e., the incorporation of organic modifier) or prepatterned substrates, is cheap and robust. As such, it represents a powerful method for fabricating highly ordered MWCNT pattern on a large area with high purity.

The gradient of stripe width is characteristic of the assembly technique applied in the present study and is closely related to the experimental conditions such as the tilt angle of the substrate, MWCNT concentration, and evaporation temperature. The effects of these experimental conditions are examined in the following sections.

Effect of Substrate Tilt Angle. In order to investigate the effect of the tilt angle of substrate on the stripe width and spacing, the MWCNT concentration and evaporation temperature (T_i) were adjusted to 10 mg/L and 60 °C, respectively, while the substrate tilt angles were systematically varied (i.e., 45, 60, and 90°). However, tilt angle below 45° is beyond the limits of present experimental capabilities. Figure 5 shows typical optical micrograph of MWCNT stripes formed on glass substrate at different tilt angles. Again, an increase in stripe width with increasing proximity to the bottom of the substrate (i.e., from location X_1 to X_2 to X_3 (Figure 2)) was obviously

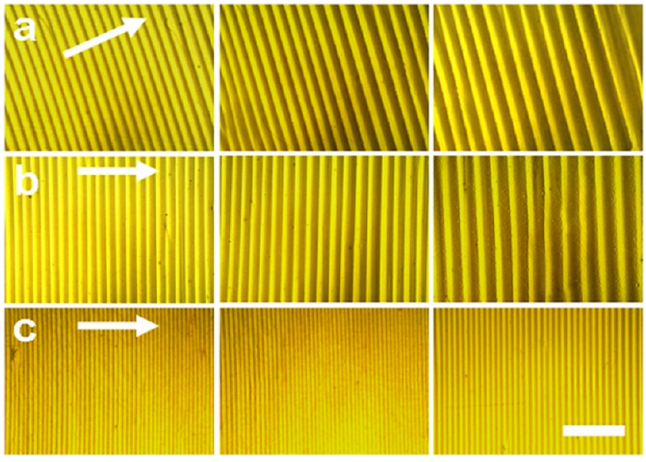

Figure 5. Optical images of MWCNTs stripe patterns formed from MWCNT concentration of 10 mg/L at T_i = 50 °C with different tilt angles of (a) 45, (b) 60, and (c) 90°. The left three images were taken from region X_1, the midterm three from X_2 and the right three from region X_3. The white arrows show the direction of stripe growth. The scale bar = 600 μm.

observed. For example, the stripe width increased progressively from 48 and 37 μm at location X_1 to 69 and 54 μm at location X_2 to 94 and 82 μm at location X_3 when the tilt angles were 45 and 60°, respectively, as shown in Figure 6. Clearly, the extent

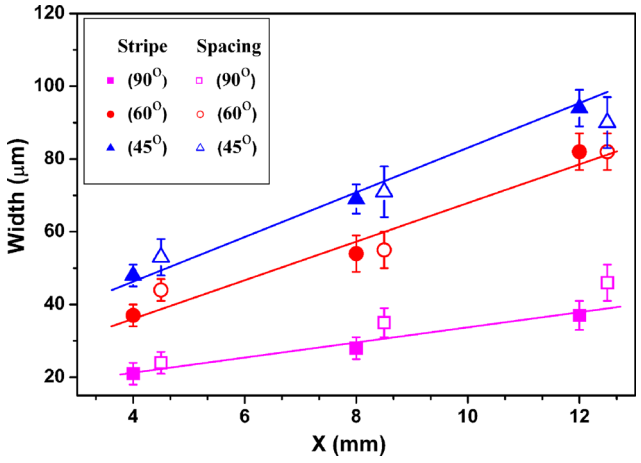

Figure 6. Effect of tilt angle on stripe width and spacing. Error bars indicate the standard deviation of the data from 5 stripes and spacing, at least 4 samples.

of this variation depends directly on the substrate tilt angle. The width of stripe at tilt angle of 45° increased much more than that at tilt angle of 60°. After further increasing the substrate tilt angle to 90°, almost no change in the stripe width was observed (i.e., stripe width is almost constant, about 30 ± 5 μm), as shown in Figures 5c and 6. On the other hand, the stripe width and spacing at the same region are also dependent on the substrate tilt angle. For example, the average stripe width and spacing at the region X_3 decreased from 94 and 90 μm to 82 and 82 μm to 37 and 46 μm, respectively, when the substrate tilt angle increased from 45 to 60 to 90° (Figure 6).

As mentioned previously, the meniscus stuck to the inclined substrate can be elongated further, and accordingly gives a longer distance than that stuck to a vertical substrate, which results in the dependence of the stripe spacing on the tilt angle of the substrate. Meanwhile, the stripe formation period on an inclined substrate is much longer than that on the vertical one, which also leads to an increase in the stripe width. Additionally, the gradual increase of the nanotube concentration due to the continued evaporation of solvent can enhance this tendency. Unfortunately, the reason for the fact that the characteristic of the stripe gradient has almost vanished at substrate tilt angle of 90° is still unclear.

Effect of MWCNT Concentration. Figure 7 shows representative optical micrographs of MWCNT stripes on glass substrate at location X_1. The internal temperature T_i and substrate tilt angle were maintained at 50 °C and 45°, respectively, while the concentration of MWCNTs was varied from 2.0 to 100 mg/L. As shown in Figure 7, stripe patterns as well as continuous film were obtained by varying the concentration of MWCNTs. Figure 7a shows the optical image prepared from the MWCNT/DCE suspension with a nanotube concentration of 2.0 mg/L, which demonstrated a stripe pattern. However, the stripe width was almost constant (i.e., 31 μm), indicating the disappearance of the gradient characteristic. When concentration was increased to 10–20 mg/L, gradient stripes were observed in Figures 7b and c, with the stripe width increasing progressively from 47 and 73 μm to

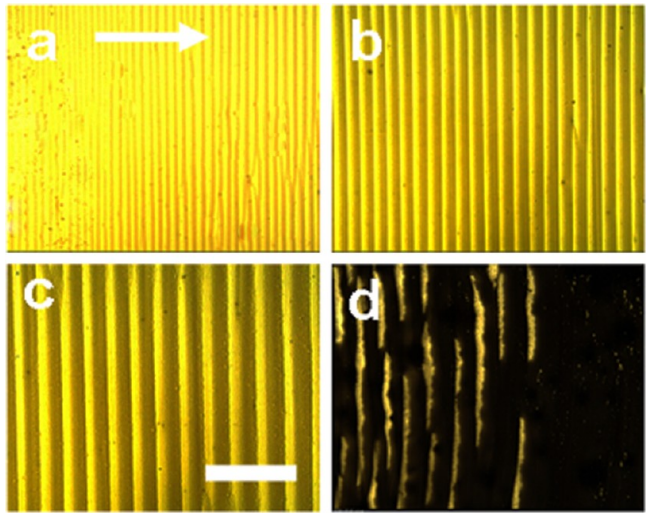

Figure 7. Optical images of stripe patterns at region X_1 formed from different MWCNT concentrations of 2.0, 10, 20, and 100 mg/L for (a–d), respectively, with the tilt angle of 45° and T_i = 60 °C. The white arrow shows the direction of stripe growth. The scale bar = 600 μm.

74 and 92 μm for MWCNT concentrations at 10 and 20 mg/L, respectively. After further increasing of the MWCNT concentration to 100 mg/L, a transition structure between the continuous film and a stripe pattern was observed as shown in Figure 7d. As expected, the number of stripes increases with decrease of MWCNT concentration. This is qualitatively natural because a higher concentration drives more nanotubes to the meniscus, where a stripe is growing, resulting in wider stripes. MWCNT concentration thus determines the nanotubes flux supplied to the stripe growing region, which is directly related to the width of the stripes.

Effect of Evaporation Temperature. Figure 8 shows representative optical micrographs of MWCNT stripes on glass substrate at location X_1. The concentration of MWCNTs and

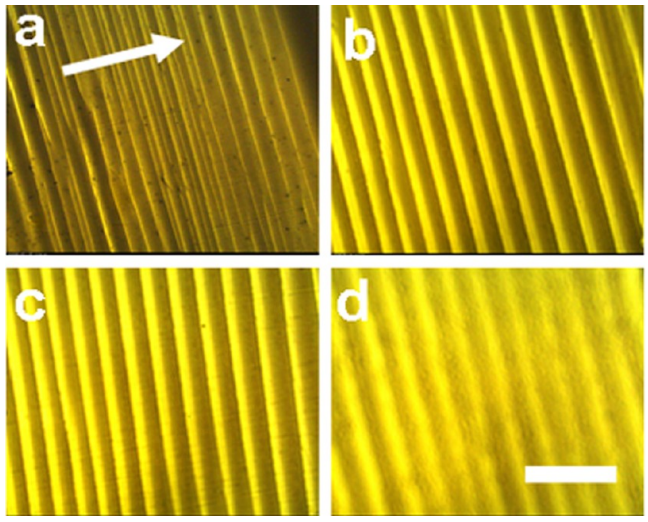

Figure 8. Optical images of MWCNT stripe patterns at region X_1 formed at different evaporation temperatures, (a) 40, (b) 50, (C) 60, and (d) 70 °C at MWCNT concentration of 20 mg/L and the tilt angle of 45°. The white arrow shows the direction of stripe growth. The scale bar = 600 μm.

dx.doi.org/10.1021/am300936a | ACS Appl. Mater. Interfaces 2012, 4, 3811–3817

substrate tilt angle were maintained at 20 mg/L and 45°, respectively, while the internal temperature T_i was varied from 40 to 70 °C. As shown in Figure 8a, although stripe patterns could be formed at T_i = 40 °C, the stripe spacing was much small, resulting in the formation of almost continuous MWCNT film. When T_i was increased to 50−60 °C, gradient stripes were observed in panels b and c in Figure 8, with the stripe width increasing progressively from 78 and 75 μm to 95 and 93 μm for T_i at 50 and 60 °C, respectively. After further increasing of the T_i to 70 °C, thinner stripes were observed as shown in Figure 8d. Generally, the increase in the evaporation temperature means a faster descent of the liquid level. Faster descent would allow fewer nanotubes to be deposited on a substrate, leading to thinner stripes.

Electrical Properties of MWCNT-FET Devices. Regular MWCNT stripe patterns can also be fabricated on other substrates such as Si/SiO_2 and polyethylene terephthalate (PET) film. In order to investigate the application of the MWCNT stripe patterns, MWCNT-FET devices were constructed by using the stripes formed on Si/SiO_2 substrate (Figure 9a). The MWCNT-FETs were fabricated with channel

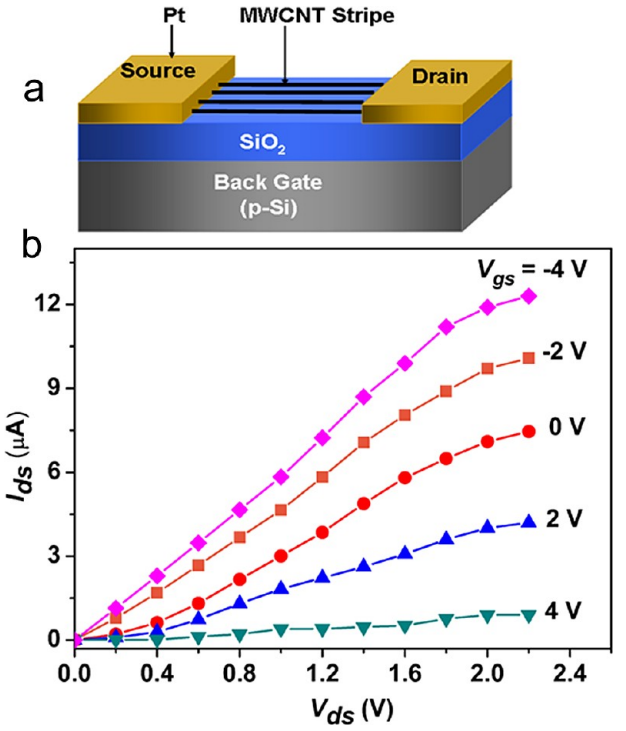

Figure 9. (a) MWCNT-FET device schematic. (b) Electrical characteristics for a typical MWCNT-FET device.

length (L_c) of 200 μm, which contained 12 MWCNT stripes at region X_1 with stripe width of around 55 μm. The electrical properties of the as-fabricated MWCNT-FET devices were measured using a semiconductor parameter analyzer. As shown in Figure 9b, the output characteristics (drain current I_{ds} versus drain voltage V_{ds}) exhibit the typical characteristics of p-channel transistors with I_{ds} being saturated at low V_{ds}. The gate voltage V_{gs} was in the range of −4 to 4 V in steps of 2 V, and V_{ds} was changed from 0 to 2.2 V in steps of 0.2 V. The current can be modulated using the underlying Si substrate as a back gate. When the V_{gs} and V_{ds} are −4 and 2.2 V, respectively, the "on" current of the FETs reaches to 1.2×10^{-5} A. The large "on" current is because of the coexistence of metallic MWCNTs. Nevertheless, the as-fabricated MWCNT stripes indicate typical p-type transistor behavior and have an on/off ratio around 100. We fabricated 15 devices and 9 of them showed FET character.

CONCLUSION

In summary, we have successfully prepared gradient stripe patterns of multiwalled carbon nanotubes over large areas by using an evaporation-induced self-assembly method and investigated the formation process systematically by varying several experimental parameters such as substrate tilt angle, nanotube concentration, and evaporation temperature. Gradient stripe patterns are spontaneously formed only when the substrate tilt angle, nanotube concentration, and evaporation temperature are in the range of 45−60°, 10−20 mg/L, and 50−60 °C, respectively. Stripe patterns prepared in the present study show a quite high degree of order. This method represents a significant advance in creating regularly organized, complex structures with potential applications in microelectronics.

AUTHOR INFORMATION

Corresponding Author

*Tel.: +86 731 58298572. Fax: +86 731 58293264. E-mail address: lihuaming@xtu.edu.cn (H.L.), gydx.1027@163.com (Y.G.).

Notes

The authors declare no competing financial interest.

ACKNOWLEDGMENTS

Financial support from NSFC (51072172), and International Joint Research Program of Hunan Province (2010WK2009) is greatly acknowledged.

REFERENCES

(1) Park, J. U.; Meitl, M. A.; Hur, S. H.; Usrey, M. L.; Strano, M. S.; Kenis, P. J. A.; Rogers, J. A. *Angew. Chem., Int. Ed.* **2006**, *45*, 581−585.
(2) Opatkiewicz, J.; LeMieux, M. C.; Bao, Z. *ACS Nano* **2010**, *4*, 2975−2978.
(3) Bradley, K.; Gabriel, J. C. P.; Gruner, G. *Nano Lett.* **2003**, *3*, 1353−1355.
(4) Ishikawa, F. N.; Chang, H.; Ryu, K.; Chen, P.; Badmaev, A.; Gomez De Arco, L.; Shen, G.; Zhou, C. *ACS Nano* **2009**, *3*, 73−79.
(5) Baughman, R. H.; Zakhidov, A. A.; De Heer, W. A. *Science* **2002**, *297*, 787−792.
(6) Kong, J.; Chapline, M. G.; Dai, H. *Adv. Mater.* **2001**, *13*, 1384−1386.
(7) Stampfer, C.; Helbling, T.; Obergfell, D.; Schöberle, B.; Tripp, M. K.; Jungen, A.; Roth, S.; Bright, V. M.; Hierold, C. *Nano Lett.* **2006**, *6*, 233−237.
(8) Weitz, R. T.; Zschieschang, U.; Effenberger, F.; Klauk, H.; Burghard, M.; Kern, K. *Nano Lett.* **2007**, *7*, 22−27.
(9) Choi, W.; Chung, D.; Kang, J.; Kim, H.; Jin, Y.; Han, I.; Lee, Y.; Jung, J.; Lee, N.; Park, G. *Appl. Phys. Lett.* **1999**, *75*, 3129−3131.
(10) Fan, S.; Chapline, M. G.; Franklin, N. R.; Tombler, T. W.; Cassell, A. M.; Dai, H. *Science* **1999**, *283*, 512−514.
(11) Nilsson, L.; Groening, O.; Emmenegger, C.; Kuettel, O.; Schaller, E.; Schlapbach, L.; Kind, H.; Bonard, J. M.; Kern, K. *Appl. Phys. Lett.* **2000**, *76*, 2071−2073.
(12) Kang, S. J.; Kocabas, C.; Ozel, T.; Shim, M.; Pimparkar, N.; Alam, M. A.; Rotkin, S. V.; Rogers, J. A. *Nat. Nanotechnol.* **2007**, *2*, 230−236.
(13) Wang, Y.; Rybczynski, J.; Wang, D. Z.; Kempa, K.; Ren, Z. F.; Li, W. Z.; Kimball, B. *Appl. Phys. Lett.* **2004**, *85*, 4741−4743.
(14) Huang, S.; Dai, L.; Mau, A. W. H. *J. Phys. Chem. B* **1999**, *103*, 4223−4227.

(15) Zheng, G.; Zhu, H.; Luo, Q.; Zhou, Y.; Zhao, D. *Chem. Mater.* **2001**, *13*, 2240−2242.
(16) Rao, S. G.; Huang, L.; Setyawan, W.; Hong, S. *Nature* **2003**, *425*, 36−37.
(17) Gao, J.; Yu, A.; Itkis, M. E.; Bekyarova, E.; Zhao, B.; Niyogi, S.; Haddon, R. C. *J. Am. Chem. Soc.* **2004**, *126*, 16698−16699.
(18) Chung, J.; Lee, K. H.; Lee, J.; Ruoff, R. S. *Langmuir* **2004**, *20*, 3011−3017.
(19) Yan, Y. H.; Li, S.; Chen, L. Q; Chan-Park, M. B; Zhang, Q. *Nanotechnology* **2006**, *17*, 5696−5701.
(20) Druzhinina, T.; Hoeppener, S.; Schubert, U. S. *Adv. Mater.* **2011**, *23*, 953−970.
(21) Ren, Z. F.; Huang, Z. P.; Xu, J. W.; Wang, J. H.; Bush, P.; Siegal, M. P.; Provencio, P. N. *Science* **1998**, *282*, 1105−1107.
(22) Sohn, J. I.; Lee, S.; Song, Y. H.; Choi, S. Y.; Cho, K. I.; Nam, K. S. *Appl. Phys. Lett.* **2001**, *78*, 901−903.
(23) Huang, S.; Mau, A. W. H.; Dai, L. *Adv. Mater.* **2002**, *14*, 1140−1143.
(24) Alvarez, N. T.; Orbaek, A.; Barron, A. R.; Tour, J. M.; Hauge, R. H. *ACS Appl. Mater. Inter.* **2010**, *2*, 15−18.
(25) Krishnan, R.; Nguyen, H. Q.; Thompson, C. V.; Choi, W. K.; Foo, Y. L. *Nanotechnology* **2005**, *16*, 841−845.
(26) Meitl, M. A.; Zhou, Y.; Gaur, A.; Jeon, S.; Usrey, M. L.; Strano, M. S.; Rogers, J. A. *Nano Lett.* **2004**, *4*, 1643−1647.
(27) Han, K. N.; Li, C. A.; Bui, M. P.; Seong, G. H. *Langmuir* **2010**, *26*, 598−602.
(28) Choi, K.; Bourgoin, J.; Auvray, S.; Esteve, D.; Duesberg, G.; Roth, S.; Burghard, M. *Surf. Sci.* **2000**, *462*, 195−202.
(29) Hong, S. W.; Jeong, W.; Ko, H.; Kessler, M. R.; Tsukruk, V. V.; Lin, Z. *Adv. Funct. Mater.* **2008**, *18*, 2114−2122.
(30) Im, J.; Kang, J.; Lee, M.; Kim, B.; Hong, S. *J. Phys. Chem. B* **2006**, *110*, 12839−12842.
(31) Tsukruk, V. V.; Ko, H.; Peleshanko, S. *Phys. Rev. Lett.* **2004**, *92*, 065502.
(32) Saran, N.; Parikh, K.; Suh, D. S.; Munoz, E.; Kolla, H.; Manohar, S. K. *J. Am. Chem. Soc.* **2004**, *126*, 4462−4463.
(33) Banerjee, S.; Hemraj-Benny, T.; Wong, S. S. *Adv. Mater.* **2005**, *17*, 17−29.
(34) Gruner, G. *J. Mater. Chem.* **2006**, *16*, 3533−3539.
(35) Widenkvist, E.; Li, J.; Jansson, U.; Grennberg, H. *Carbon* **2007**, *45*, 2732−2736.
(36) Liu, J.; Casavant, M. J.; Cox, M.; Walters, D. A.; Boul, P.; Lu, W.; Rimberg, A. J.; Smith, K. A.; Colbert, D. T.; Smalley, R. E. *Chem. Phys. Lett.* **1999**, *303*, 125−129.
(37) Hannon, J. B.; Afzali, A.; Klinke, C.; Avouris, P. *Langmuir* **2005**, *21*, 8569−8571.
(38) Jung, M. S.; Jung, S. O.; Jung, D. H.; Ko, Y. K.; Jin, Y. W.; Kim, J.; Jung, H. T. *J. Phys. Chem. B* **2005**, *109*, 10584−10589.
(39) Wakamatsu, N.; Takamori, H.; Fujigaya, T.; Nakashima, N. *Adv. Funct. Mater.* **2009**, *19*, 311−316.
(40) Kordás, K.; Mustonen, T.; Tóth, G.; Jantunen, H.; Lajunen, M.; Soldano, C.; Talapatra, S.; Kar, S.; Vajtai, R.; Ajayan, P. M. *Small* **2006**, *2*, 1021−1025.
(41) Choi, S.-W.; Kang, W.-S.; Lee, J.-H.; Najeeb, C. K.; Chun, H.-S.; Kim, J.-H. *Langmuir* **2010**, *26*, 15680−15685.
(42) Li, S.; Yan, Y.; Liu, N.; Chan-Park, M. B.; Zhang, Q. *Small* **2007**, *3*, 616−621.
(43) Huang, S.; Mau, A. W. H.; Turney, T. W.; White, P. A.; Dai, L. *J. Phy. Chem. B* **2000**, *104*, 2193−2196.
(44) Kamat, P. V.; Thomas, K. G.; Barazzouk, S.; Girishkumar, G.; Vinodgopal, K.; Meisel, D. *J. Am. Chem. Soc.* **2004**, *126*, 10757−10762.
(45) Tumpane, J.; Karousis, N.; Tagmatarchis, N.; Nordén, B. *Angew. Chem., Int. Ed.* **2008**, *47*, 5148−5152.
(46) Li, Y.; Xu, C.; Wei, B.; Zhang, X.; Zheng, M.; Wu, D.; Ajayan, P. M. *Chem. Mater.* **2002**, *14*, 483−485.
(47) Shimoda, H.; Oh, S. J.; Geng, H. Z.; Walker, R. J.; Zhang, X. B.; McNeil, L. E.; Zhou, O. *Adv. Mater.* **2002**, *14*, 899−901.
(48) Engel, M.; Small, J. P.; Steiner, M.; Freitag, M.; Green, A. A.; Hersam, M. C.; Avouris, P. *ACS Nano* **2008**, *2*, 2445−2452.
(49) Zeng, H.; Kristiansen, K.; Wang, P.; Bergli, J.; Israelachvili, J. *Langmuir* **2011**, *27*, 7163−7167.
(50) Watanabe, S.; Inukai, K.; Mizuta, S.; Miyahara, M. T. *Langmuir* **2009**, *25*, 7287−7295.
(51) Yang, M.; Gao, Y.; Li, H.; Adronov, A. *Carbon* **2007**, *45*, 2327−2333.
(52) Lin, Y.; Su, Z.; Xiao, G.; Balizan, E.; Kaur, G.; Niu, Z.; Wang, Q. *Langmuir* **2011**, *27*, 1398−1402.